Automatic Synthesis of Cine Viability MRI Images for Evaluation of Coronary Heart Disease

Azza S. Hassanein, Ayman M. Khalifa, Walid Al-Atabany, and Mohamed T. El-Wakad, Brian Shapiro, and El-Sayed H. Ibrahim

Abstract— **Coronary heart disease (CHD) is the leading cause of death worldwide. Cardiac magnetic resonance imaging (MRI) is a valuable imaging modality, as it can noninvasively provide information about myocardial function, viability, and morphology. Viability delayed-enhancement (DE) images are acquired at a single timeframe while myocardial functional (tagged) images are acquired as a cine loop of timeframes throughout the cardiac cycle. In this work, we propose a method for estimating DE images at all timeframes in the cardiac cycle without additional scan time to show both viability and functional information in the same image. The method is based on generating a dense motion field of the heart from the acquired tagged images, and then applying the extracted field to the acquired DE image. The developed technique is accurate in generating cine DE images and providing simultaneous information about myocardial viability and wall motion for comprehensive patient evaluation and optimal treatment selection.**

I. Introduction

Coronary heart disease (CHD) is the leading cause of death worldwide with huge cost associated with treatment and prevention [1]. In this disease, a branch or more of the coronary artery is hardened and narrowed due to the build up of plaque that can rupture and block blood supply to the myocardium causing infarction in the affected regions.

A typical cardiovascular MRI exam for evaluating CHD includes cine, tagging, and delayed-enhancement (DE) sequences to produce images for evaluating global heart function (e.g. ejection fraction and myocardial mass), myocardial contractility, and tissue viability, respectively [2]. Combining the information from these sequences allows the physician to comprehensively evaluate the heart condition and determine the right treatment. The MRI cine images provide movies that show the heart motion during the cardiac cycle for visual assessment of heart morphology and wall motion, and quantitative evaluation of global function [3].

MRI tagging is a well-known technique used for analyzing regional heart motion [4]. In this technique, a pattern of spatially saturated magnetism is embedded on the myocardium at end diastole. The tagging pattern deforms according to the heart motion during the cardiac cycle, which can then be analyzed to obtain measures of myocardial deformation, e.g. strain, strain rate, and torsion .

DE imaging is of special importance for identifying myocardial infarction (MI), as infarcted myocardium appears hyper-enhanced (bright) 10-15 minutes after intravenous administration of gadolinium (Gd) contrast agent. Gadolinium has the effect of shortening the tissue longitudinal relaxation time, which results in signal enhancement on T1-weighted images [5]. DE imaging is acquired in one breath-hold during mid-diastole when the heart undergoes minimal motion [6].

Obtaining cine viability images is desirable as it would allow for evaluating both wall motion and viability at the same time from a single set of images without misregistration problems. However, acquisition of cine viability images is challenging, as the DE pulse sequence has to be repeatedly applied at different phases through the cardiac cycle. The limitation of this approach is that it entails increasing the scan time with the possibility of variable tissue enhancement between different images as time elapses post Gd injection.

In this study, we propose a new technique to synthesize cine viability images throughout the cardiac cycle by extracting the motion field of the heart from the cine tagged images, and use it to guide creation of new DE timeframes based on the acquired DE image at mid-diastole. We compare different methods for extracting the motion field from the MRI tagged images to determine the best method for the developed technique.

II. Methodology

A. Motion field estimation

Myocardial motion estimation was performed using different techniques to obtain the motion field between different timeframes of the tagged images. In this study, we focused on the following techniques:

1. HARP: Harmonic phase (HARP) is a widely used technique for extracting and processing motion information from tagged MRI images [7]. This technique filters the first two harmonic peaks in the Fourier domain of the tagged image (k-space) and uses them to calculate phase images (called HARP images) using inverse Fourier transform. HARP tracks motion based on the fact that the phase value of any material point does not change with time.

2. Optical Flow (OF): OF is a well-established motion tracking technique in computer vision [8]. The goal here is to calculate the motion between two images under the assumption that the brightness of material points does not change with time as they move. This assumption provides the brightness constraint equation:

A. S. Hassenein is with Helwan University, Cairo, Egypt (e-mail: azza.sayed@helwan.edu.eg).
A. M. Khalifa is with Helwan University, Cairo, Egypt (e-mail: aymankhalifa2002@yahoo.com).
W.Al-Atabany is with Helwan University, Cairo, Egypt (e-mail: atabany@yahoo.com).
M. T. El-Wakad is with Helwan University, Cairo, Egypt (e-mail: mtwakad@yahoo.com).
B. Shapiro is with Mayo Clinic, Jacksonville, FL, USA (e-mail: shapiro.brian@mayo.edu).
E. H. Ibrahim is with Mayo Clinic, Jacksonville, FL, USA (e-mail: ibrahim.elsayed@mayo.edu).

978-1-4244-7929-0/14/$26.00 ©2014 IEEE

$$I_x u + I_y v + I_t = 0 \quad (1)$$

, where $I, I_x I_y$, and I_t represent the image signal intensity and its derivatives with respect to x, y, and t, respectively.

There are several techniques that compute the optical flow field; such as Lucas-Kanade (LKOF), Horn-Shunck (HSOF), and band-pass (BPOF) algorithms [9] which are included in this study.

2.1 LKOF: LKOF assumes that the motion vectors are constant at any region but shift from one position to another. Assuming that flow (V_x , V_y) is constant in a small window centered at a point (x, y) and has size of $m \times m$, and the pixels of the window are numbered as $i = 1 \ldots n$, then flow can be obtained by solving the generated set of equations using the least squares method:

$$\begin{bmatrix} V_x \\ V_y \end{bmatrix} = \begin{bmatrix} \sum I_{x_i}^2 & \sum \mathrm{I}_{x_i}\mathrm{I}_{y_i} \\ \sum \mathrm{I}_{x_i}\mathrm{I}_{y_i} & \sum I_{y_i}^2 \end{bmatrix}^{-1} \begin{bmatrix} -\sum \mathrm{I}_{x_i}\mathrm{I}_{t_i} \\ -\sum \mathrm{I}_{y_i}\mathrm{I}_{t_i} \end{bmatrix} \quad (2)$$

By solving equation (2) for each image pixel, the motion field can be calculated [10]

2.2 HSOF: HSOF assumes that the velocity field in the image varies smoothly. Thus, the estimated velocity values are calculated based on this constraint [10]. To achieve that, a global energy function is formulated that can be minimized to obtain the optimal velocity value. The results of this minimization are velocities calculated iteratively using:

$$V_x^{\boldsymbol{k+1}} = \overline{V}_x^{\boldsymbol{k}} - \frac{\boldsymbol{I_x(I_x\overline{V}_x^{k} + I_y\overline{V}_y^{k} + I_t)}}{\boldsymbol{\alpha^2 + I_x^2 + I_y^2}} \quad (3)$$

$$V_y^{\boldsymbol{k+1}} = \overline{V}_y^{\boldsymbol{k}} - \frac{\boldsymbol{I_y(I_x\overline{V}_x^{k} + I_y\overline{V}_y^{k} + I_t)}}{\boldsymbol{\alpha^2 + I_x^2 + I_y^2}} \quad (4)$$

, where k is the iteration number, α is regularization constant that leads to smoother velocities for larger values, $\overline{V}_x$and $\overline{V}_y$ are the weighted average of the x and y velocity components calculated in the neighborhood of pixel at location (x, y).

2.3 BPOF: BPOF estimates the velocity by representing the tagged images as a 2D sinusoidal pattern that modulates the underlying brightness field. Thus, in the frequency space, the images consist of various sub-bands located at frequencies related to the product of sinusoidal frequencies [11]. To extract these sub-bands, a circular bandpass filter is applied at the locations of the first harmonic peaks in the horizontal, vertical, diagonal, and back diagonal directions.

The velocity is calculated from all sub-bands in order to provide a robust solution without the need for a regularization parameter or iterations. In order to estimate the velocity from each sub-band image, the velocity field is assumed to be locally constant, which is mathematically equivalent to nulling the spatial derivatives of equation (1) at all pixels:

$$\mathrm{I}_{xx}^i u + I_{xy}^i v + I_{tx}^i = 0 \ , \qquad i = 1,2,3,4 \quad (5)$$

$$\mathrm{I}_{xy}^i u + I_{yy}^i v + I_{ty}^i = 0 \ , \qquad i = 1,2,3,4 \quad (6)$$

, where i is the sub-band number. The set of Equations (1),(5), (6) form a system of equations that can be written as:

$$A.v = -b \quad (7)$$

, where

$$A = \begin{bmatrix} I_x^1 & I_{xx}^1 & I_{yx}^1 & I_x^2 & I_{xx}^2 & I_{yx}^2 & I_x^3 & I_{xx}^3 & I_{yx}^3 & I_x^4 & I_{xx}^4 & I_{yx}^4 \\ I_y^1 & I_{xy}^1 & I_{yy}^1 & I_y^2 & I_{xy}^2 & I_{yy}^2 & I_y^3 & I_{xy}^3 & I_{yy}^3 & I_y^4 & I_{xy}^4 & I_{yy}^4 \end{bmatrix}^T$$

$$, v = [V_x \quad V_y]^T$$

$$, b = \begin{bmatrix} I_t^1 & I_{xt}^1 & I_{yt}^1 & I_t^2 & I_{xt}^2 & I_{yt}^2 & I_t^3 & I_{xt}^3 & I_{yt}^3 & I_t^4 & I_{xt}^4 & I_{yt}^4 \end{bmatrix}^T$$

This system of equations is overdetermined, and the velocity components are calculated using the pseudo-inverse method.

B. Numerical Phantom Design

A synthetic sequence of images was created to evaluate the accuracy of estimating the motion field from the tagged images using the methods described in the previous section. This sequence consists of 25 images of size 256×256 pixels and Field of View = 145×145 mm^2 to represent different timeframes during the cardiac cycle. Each image contains an annular object to represent a short-axis view of a basal slice of the left ventricle with inner (endocardial) and outer (epicardial) radii of 30 mm and 40 mm, respectively, at end diastole (Fig. 1-a). The tag spacing was set to 7mm with 70% duty cycle D, and tags tilted by 45° from the x-axis (Fig. 1-b). The tagging pattern is modeled according to the formula:

$$I_{tag}(x,y) = \left[AD + \sum_{n=1}^{3} \frac{2A}{n\pi} \sin\left(\frac{n\omega D}{2}\right) \cos(n\omega \boldsymbol{x})\right] \cdot \left[AD + \sum_{n=1}^{3} \frac{2A}{n\pi} \sin\left(\frac{n\omega D}{2}\right) \cos(n\omega \boldsymbol{y})\right] \quad (8)$$

, where $I_{tag}(x,y)$ is the pixel intensity, A is the amplitude of the sinusoidal signal, ω is the fundamental frequency of the 2D sinusoidal signal, x is pixel position in the horizontal direction, and y is pixel position in the vertical direction, D is the duty cycle, and n is the number of harmonics used.

This tag pattern is multiplied by the myocardium to generate a numerical phantom for tagged MRI images (Fig. 1-c). The motions considered in this study are radial expansion, radial contraction, and rotation, taken with values close to real heart motion (Fig. 2). The synthetic image sequence is considered the ground truth for evaluating motion estimation error for different motion tracking methods.

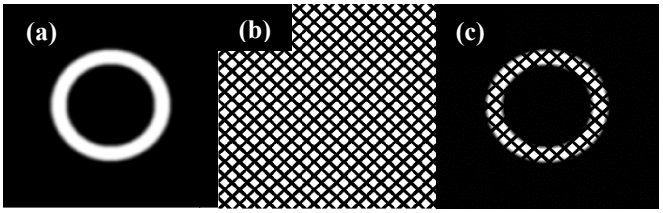

Figure 1. (a) Circular disc represents the myocardium, (b) SPAMM tag pattern, and (c) Myocardium numerical phantom.

C. Motion-Guided Cine DE Imaging

The datasets used in this work was acquired from 4 patients with MI imaged on a 3.0T MRI scanner. Each dataset is composed of a sequence (22 timeframes) of short-axis tagged MRI images and the corresponding DE single frame image acquired at mid-diastole. Cine short-axis images were also acquired for reference. The motion field was estimated from the tagged images using the methods described in section II. A , as illustrated in Figure 3. The

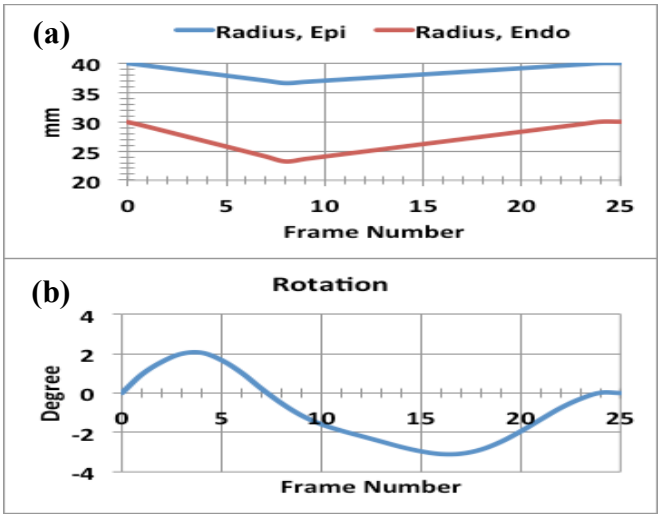

Figure 2. (a) Epicardial and endocardial radii of the numerical phantom during the cardiac cycle, (b) Myocardial rotation during the cardiac cycle.

extracted motion field was used to reconstruct the cine DE images starting from the acquired (known) DE image. The BPOF algorithm resulted in lowest estimation error, as shown in the results; therefore, it was used for motion estimation in the patient images.

D. Image Processing and Analysis

Custom software was built in Matlab to implement the developed algorithms. Myocardial thickening was measured by manual segmentation of both cine and cine DE images by an expert. The hyper-enhanced region in DE images was identified using full-width at half-maximum method. Circumferential strain was measured from the tagged images using the HARP technique.

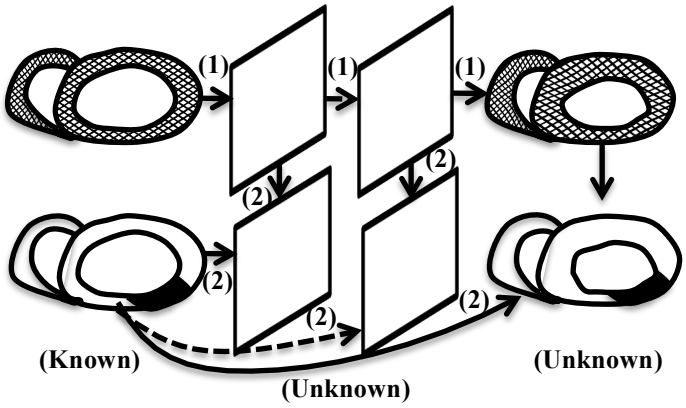

Figure 3. Processing steps of the proposed algorithm. Arrows with number 1 indicate the first step: extracting the motion field. Arrows with number 2 indicate the second step: combining the extracted motion field and acquired (known) DE frame to estimate other DE frames at different heart phases.

III. RESULTS

A. Numerical Simulation

Figure 4 shows the meshes (contours) drawn at end diastole (initial frame) with tracking at end systole using HARP and BPOF. HARP provides good tracking results for mid-wall , but suffers from errors at the boundaries. BOP provides optimal tracking for all points. Figure 5 shows the

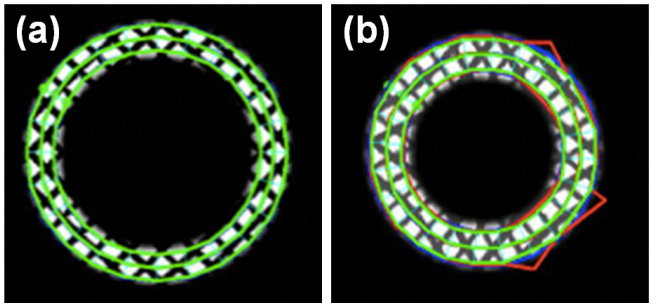

Figure 4, Mesh tracking at (a) end diastole (initial time frame) and (b) end systole using BPOF (Green) and HARP (Red) compared to actual tracking (Blue).

average error in tracking points at epicardium (EPI), mid-wall (MED), and endocardium (ENDO) using the different techniques: HARP, LKOF, HSOF, and BPOF. The error curves confirm the results in Figure 4. HARP tracking errors are considerable at all cardiac phases on the epicardium and at mid-to-late diastole on the endocardium. Among the different optical flow techniques, HSOF has the worst tracking errors, especially on the epicardium during systole. LKOF and BPOF have similar error patterns, with overall error from BPOF smaller than LKOF, especially at mid-wall.

B. Patient results

Figure 6 shows sample cine images of a mid-ventricular slice at end diastole and end systole from, along with the corresponding synthetic DE images obtained with the BPOF technique. The DE images show changes in the MI shape

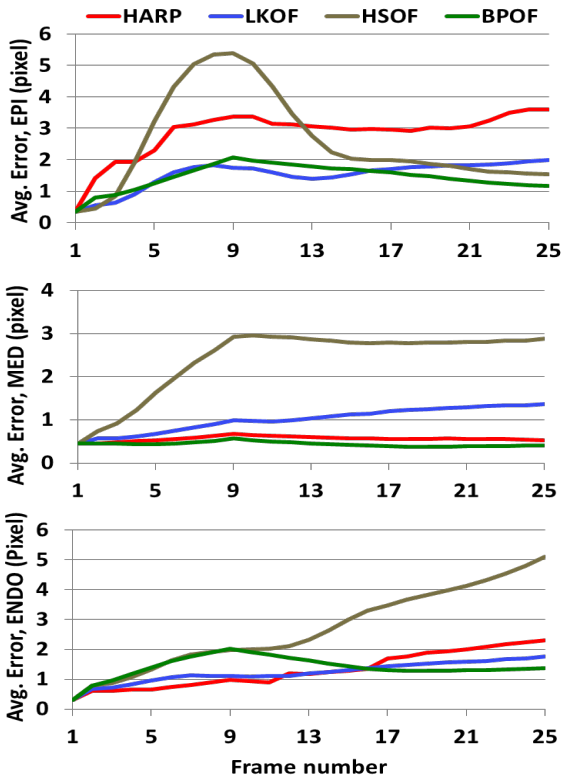

Figure 5. Average tracking Error at (a) epicardium (EPI), (b) mid-wall of the left ventricle (MED), and (c) endocardium (ENDO) using different motion field estimation techniques: HARP, LKOF, HSOF, and BPOF.

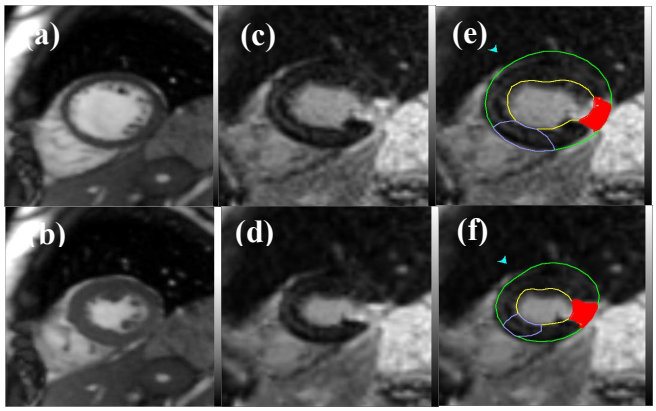

Figure 6. MRI Cine images at (a) end diastole and (b) end systole, as well as the corresponding synthetic DE images (c,d). Palettes (e) and (f) show the DE regions (red) and wall thickening for the two synthetic DE images.

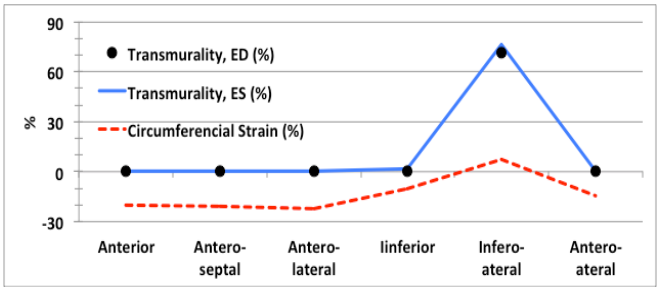

Figure 7. MI transmurality at end diastole (blue) and end systole (black dots) for different regions. The red dashed curve shows circumferential strain at the same regions calculated from the tagged images.

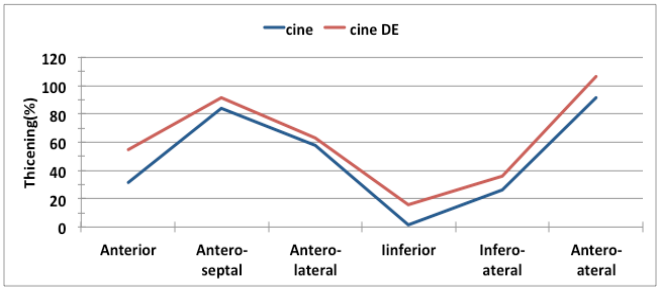

Figure 8. Wall thickening at different regions using cine (blue) and synthetic DE (red) images.

(in red) and myocardial thickening during the cardiac cycle. Figure 7 shows MI transmurality (measured from synthetic DE images) and circumferential strain (calculated from the tagged images) at different regions in the slice shown in Figure 6. The results show excellent agreement between myocardial thickening and strain. The region with maximum MI transmurality and lowest strain agrees with MI location as shown in Figure 6. Figure 8 shows wall thickening calculated for the slice in Figure 6 using original cine and synthetic cine DE images. The results show excellent agreement between measurements from both sequences.

IV. Discussion and Conclusion

In this paper, we evaluated different motion field estimation techniques for tracking tagged MRI images. The BPOF technique showed minimal tracking error. While tracking accuracy with BPOF is close to HARP at the mid-wall regions, it is significantly better at the epicardium and endocardium where HARP fails to track points near the left ventricular boundaries.

The developed technique for generating cine DE images shows both viability and wall motion at the same time with additional scan time or misregistration errors, which is important for comprehensive evaluation of the patient's condition and determining optimal treatment strategy, for example identifying candidates for revascularization therapy based on contractility reserve and MI transmurality. Further, the generated composite images would be useful for differentiating between Gd recess in the muscle and actual myocardial scar, a process that is usually performed by comparing cine and DE images side-by-side.

Despite the encouraging results in this work, more patients with different degrees of MI need to be studied to establish the clinical importance of the developed technique, especially with the possibility of viability imaging at various heart phases. Future work also includes generalizing the developed technique for 3D analysis.

Acknowledgment

This work is partially supported by a research and development grant (PDP2012.R12.4) from ITIDA agency, Ministry of Communication and Information Tech., Egypt.

References

[1] J. J. McMurray and M. A. Pfeffer, "Heart Failure," Lancet, vol. 365, no. 9474, pp. 1877-1889, May 2005.

[2] E. H. Ibrahim, "Imaging Sequences in Cardiovascular Magnetic Resonance: Current Role, Evolving Applications, and Technical Challenges," International Journal of Cardiovascular Imaging, vol. 28, no. 8, pp. 2027-2047, 2012.

[3] Zur Y, Wood ML, Neuringer LJ. Motion-insensitive, steady-state free precession imaging. Magn Reson Med 1990;16:444–459.

[4] E. H. Ibrahim, "Myocardial Tagging by Cardiovascular Magnetic Resonance: Evolution of Techniques-Pulse Sequences, Analysis Algorithms, and Applications," Journal of Cardiovascular Magnetic Resonance: Official Journal of the Society of Cardiovascular Magnetic Resonance, vol. 28, pp. 13-36, Jul 2011.

[5] J. Oshinski , Z. Yang, J. Jones and J. Mata, "Imaging Time after Gd-DTPA Injection is Critical in Using Delayed Enhancement to Determine Infarct Size Accurately with Magnetic Resonance Imaging," Circulation, 2001.

[6] R. Kim, D. Shah, R. Judd, "How we perform delayed enhancement imaging," J Cardiovasc. Magn. Reson. 2003; 5:505-514

[7] N. Osman, E. McVeigh and J. Prince, " Imaging Heart Motion Using Harmonic Phase MRI," IEEE Trans Med Imaging , vol. 19, no. 3, p. 186–202, 2000.

[8] J. L. Barron, D. J. Fleet and S. S. Beauchemin, "Performance of Optical Flow Techniques," International Journal of Computer Vision, vol. 12, p. 43–77, 1994.

[9] J. L. Barron, D. J. Fleet and S. S. Beauchmin, "Systems and Experiment Performance of Optical Flow Techniques," International Journal of Computer Vision, vol. 12, no. 1, pp. 43-77, 1994.

[10] Horn, B.K.P. and B.G. Schunck, Determining Optical Flow. Artificial Intelligence, 1981. 17: p. 185–204.

[11] Prince, J.L., S.N. Gupta, and N.F. Osman, Bandpass Optical Flow for Tagged MRI. Medical Physics, 2000. 27: p.108–118.